Kuramoto-type phase transition with metronomes

Sz Boda, Sz Ujvári, A Tunyagi and Z Néda

Department of Physics, Babeş-Bolyai University, RO-400084, Cluj-Napoca, Romania

E-mail: zneda@phys.ubbcluj.ro

Abstract

Metronomes placed on the perimeter of a disc-shaped platform, which can freely rotate in a horizontal plane, are used for a simple classroom illustration of the Kuramoto-type phase transition. The rotating platform induces a global coupling between the metronomes, and the strength of this coupling can be varied by tilting the metronomes' swinging plane relative to the radial direction on the disc. As a function of the tilting angle, a transition from spontaneously synchronized to unsynchronized states is observable. By varying the number of metronomes on the disc, finite-size effects are also exemplified. A realistic theoretical model is introduced and used to reproduce the observed results. Computer simulations of this model allow a detailed investigation of the emerging collective behaviour in this system.

(Some figures may appear in colour only in the online journal)

1. Introduction

Synchronization is the emergence of coherent dynamics in ensembles of interacting and self-sustaining elements with periodic motion. In the case of oscillators this phenomenon is observable as an adjustment of their rhythms due to a weak phase difference minimizing interaction between them. Synchronization usually appears as a phase-locking scenario, and the synchronized state is a stable limit cycle of the system [1–6]. Synchronization of totally identical oscillators with a phase difference minimizing interaction between them is easily imaginable. Because in real life one cannot find two totally identical oscillators, the real challenge lies in understanding synchronization in ensembles of non-identical units, where each oscillator has its own natural frequency.

The earliest known study of spontaneous synchronization between coupled non-identical oscillators dates back to 1657, when Christian Huygens studied the motion of maritime clocks. Due to the practical challenges, these devices were built using two clocks operating simultaneously and in such a way that if one clock stopped, the other one was able to provide timekeeping. This setup made it possible for him to discover *an odd kind of sympathy* because in his clocks, which were suspended side by side, the pendulums swung at the same frequency and 180° out of phase. After perturbing the system, the anti-phase synchronized motion

resumed. Driven by his scientific curiosity, he performed a series of controlled experiments, and concluded that this strange phenomenon occurs due to small vibrations transmitted through the clocks' common suspension frame. He summarized his study in a letter to the Royal Society of London [7], and this letter is the earliest known scientific discussion of the phenomenon of synchronization. Recently, several research groups revisited Huygens's original experiment and for an excellent review we suggest the work of Kapitaniak *et al* [8].

A more general approach to the fascinating synchronization phenomenon of non-identical oscillators was pioneered by Winfree. In 1966, as a graduate student at Princeton University, he began to study coupled oscillator systems. Based on many experimental observations in real systems, he proposed a novel modelling framework for explaining the emergence of synchronization in large populations of coupled self-sustained oscillators, with a probabilistic spread of their natural frequencies. He found that synchronization appears as a phase transition when the coupling strength is increased above a critical limit [9]. Inspired by Winfree's work, a few years later Kuramoto and Nishikava reformulated and simplified this model in order to make it analytically solvable [2]. They established one of the most successful and well known models for understanding the synchronization of an ensemble of non-identical and globally coupled oscillators. The key for getting an analytical solution was to choose a proper harmonic form for the coupling. For a normal distribution of the oscillators' natural frequencies, their model, which is known today as the Kuramoto model, yields the critical coupling strength at which collective rhythm emerges. The Kuramoto model is exactly solvable for uniform and global coupling between the oscillators, and serves nowadays as a textbook example in statistical physics for exemplifying and teaching second-order phase transitions. Therefore, illustration of the Kuramoto-type phase transition through classroom experiments has great pedagogical value.

Panteleone [10] proposed in this sense a simple mechanical setup of two metronomes placed on a light, easily movable platform. From acoustic observation of the metronomes beats, he found that, for small frequency differences, the metronomes were able to synchronize, independently of the initial conditions, in a time interval of the order of tens of seconds. However, synchronization was not achieved for larger frequency differences. Pantaleone also derived approximate equations of motions for the time evolution of the metronome ensemble, using for the metronome escapement and damping a term borrowed from van der Pol oscillators [11]. He also suggested that extending the model to a multimetronome system would provide additional opportunities for observing much interesting behaviour.

As a feedback to Panteleone's work, Ulrichs *et al* [12] examined the behaviour of many (up to 100) globally coupled metronomes by using numerical simulations. For the dynamics of the coupled system they used the equations of motion derived by Pantaleone. They reported that the Kuramoto-type transition is observable in their system as well. In agreement with the observations of the real metronome system made by Pantaleone, they also confirmed the absence of anti-phase synchronization, and reported only in-phase synchronization.

This paper intends to continue the above sketched line of studies, considering a direct and straightforward experimental illustration of the Kuramoto-type phase transition for several metronomes. In our experimental setup the metronomes are arranged symmetrically on the perimeter of a freely rotating disc, as illustrated in figure 1. The rotation of the disc induced by the metronomes' beats acts as a coupling mechanism between the metronomes' phases. Continuing our previous study [13], where we examined the influence of metronome number and their nominal frequency on the observed synchronization level, we now examine the influence of the coupling strength in the system. The coupling strength is adjusted in a very simple manner by placing the metronomes at different angles with respect to the radial direction on the disc. The coupling strength will thus decrease to zero as we approach $90°$.
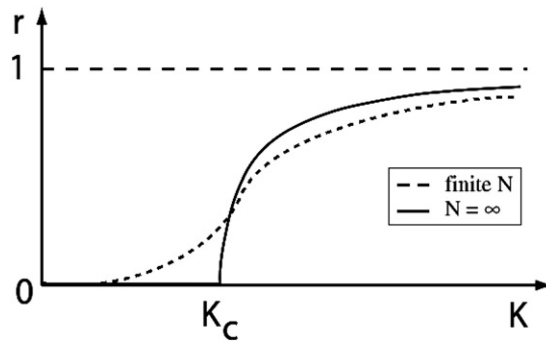
Figure 1. The order parameter of the Kuramoto model as a function of the coupling strength between the rotators. The continuous line is for a system composed of an infinite number of oscillators, the dashed line corresponds to a finite system. At $K = K_c$ an order–disorder phase transition is observable.

A realistic model with experimentally determined model parameters is used to confirm the experimentally obtained data and for extrapolating the results in the limit of hundreds of metronomes.

The rest of the paper is organized as follows. First, we briefly discuss the classical Kuramoto model and its main achievements, then we present our experimental setup and results. We consider realistic equations of motion for the dynamics of the system, and computationally investigate this model with experimentally determined model parameters. We illustrate both by experiments and simulations the appearance of the Kuramoto-type phase transition, and compare our experimental and theoretical results. We believe that the presented experiments and model are suitable for university level student projects and laboratory demonstrations and could also be of interest for specialists in the field of emerging synchronization.

2. Kuramoto model

The model is elaborated by Kuramoto and Nishikawa [2, 5], and considers an ensemble of globally coupled rotators. Each rotator i (oscillator) has its own, intrinsic ω_i frequency, which is distributed according to a $g(\omega)$ probability distribution. The dynamics of the system is given by a set of coupled first-order differential equations

$$\frac{\partial \theta_i}{\partial t} = \omega_i + \frac{K}{N} \sum_{j=1}^{N} \sin(\theta_j - \theta_i), \quad i = 1\text{--}N, \tag{1}$$

where N is the number of rotators, K is the coupling constant and θ_i is the phase of unit i. Without coupling ($K = 0$) the system decouples in a trivial manner and each rotator follows its own natural frequency, thus no synchronization is possible. The chosen harmonic form for the coupling has the effect of reducing the phase difference between the oscillators, and allows a self-consistent separation of the coupled equations. An analytic and exact solution can be obtained in the thermodynamic limit ($N \rightarrow \infty$) for the ($r \in [0, 1]$) order parameter which characterizes the level of synchronization in the system:

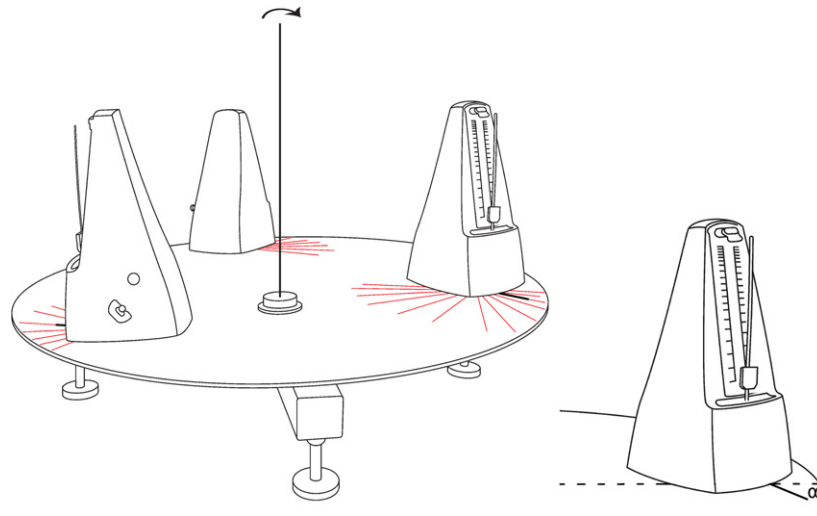$$r \exp(i\psi) = \frac{1}{N} \sum_{j=1} N \exp(i\theta_j). \tag{2}$$

Figure 2. Schematic view of the experimental setup: metronomes are placed on the perimeter of a disc that can rotate around a vertical axis. We also illustrate one metronome displaced by an angle α relative to the radial direction on the disc.

In the equation ψ represents a *collective phase* of the synchronized state. For randomly distributed θ_i phases there is no synchronization in the system and one gets $r = 0$. In the case of complete synchronization all phases are the same, and we get $r = 1$. A value $r \in (0, 1)$ indicates partial synchronization. Kuramoto and Nishikawa found that the coupled rotator system presents an order–disorder-type phase transition in the thermodynamic limit. For a given rotator ensemble, there is K_c critical coupling in the system so that for $K < K_c$ the system is in a disordered phase, the units will not synchronize, and $r = 0$ will be the stable solution. For $K > K_c$ partial synchronization appears and $r > 0$ is the stable solution. Complete synchronization ($r = 1$) appears in the $K \to \infty$ limit. For a normal distribution of the oscillator frequencies characterized by a σ standard deviation, the critical coupling is

$$K_c = \sqrt{\frac{2}{\pi^3}}\sigma. \tag{3}$$

The phase transition monitored through the r order parameter is sketched in figure 1. Results for a system composed of an infinite number of rotators are plotted with a continuous line, the results expected for finite system sizes are plotted with a dashed line.

3. Experimental setup and results

We consider a system composed of metronomes placed on a freely rotating disc-like platform. By tilting the metronomes' orientation relative to the radial direction on the disc we are able to reproduce the Kuramoto-type phase transition. A schematic view of the setup and a magnification for one metronome is sketched in figure 2.

Metronomes were patented by Johann Maelzel in 1815 as a timekeeping tool for musicians [14]. They produce regular, metrical beats, hence the native frequency unit for their beat frequency is given in beats per minute (BPM). The oscillating part of the metronome is a physical pendulum, which consists of a rod with two different weights on it (see figure 3). One of these weights is fixed at the lower end of the rod (denoted by W_1) and the other one,
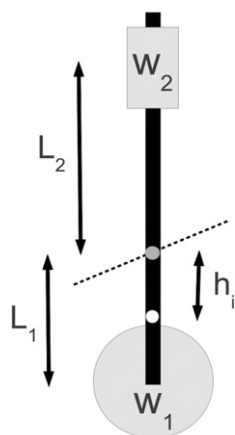
Figure 3. Schematic view of the metronome's bob with the two masses W_1 and W_2. The dotted line denotes the horizontal suspension axis, and the white dot illustrates the centre of mass of this system.

W_2, is movable and can be fixed at some marked values. In our case $W_1 > W_2$, and the rod is suspended on a horizontal axis between the two weights in a stable manner, so that the centre of its mass lies below the suspension axis.

The metronomes' frequency can be tuned by sliding the W_2 weight on the rod. The marked positions for the W_2 weight lead to oscillations with standard nominal beat frequencies ranging from 40 to 208 BPM. In order to overcome the unavoidable energy dissipation and to maintain the self-sustaining motion, the metronomes have their own exciting mechanism. This mechanism yields additional momentum to the physical pendulum in the form of pulses, delivered at a given phase of the oscillation period. The pulse given by the exciting mechanism is in the pendulum's swinging plane, and this pulse will be the main source of coupling in our system. These momenta (p) can be decomposed into two components, one parallel to the radial direction on the disc ($p_{||}$) and one perpendicular to this direction ($p_\perp$). Rotating the pendulum's swinging plane by $\alpha < 90°$ (illustrated in figure 1), the $p_\perp$ component will decrease ($p_\perp = p \cdot \cos(\alpha)$), and the $p_{||}$ component will increase ($p_{||} = p \cdot \sin(\alpha)$).

The global coupling between the metronomes is realized by the small angle oscillations of the platform. These oscillations appear as a result of the $p_\perp$ terms. We can adjust the coupling by rotating the metronomes. One can easily realize that the coupling will be maximal if $\alpha = 0$ or $\alpha = 180$, and there will be no coupling for $\alpha = 90$. The setup is thus appropriate for modeling a globally coupled oscillator system, where the coupling strength between the oscillators can be controlled. To control the tilting angles, α, of the metronomes we mounted a needle on their bottom, perpendicular to the bob's swinging plane. We used six metronomes, which were evenly spread on the perimeter of the disc, and for each of the positions we marked with red lines well-defined α angles, ranging from 0° to 180° with a step of 15°. This is illustrated both in the schematic setup from figure 2 and in the photo of our experimental apparatus in figure 4(a).

In the experiments we used commercially available Thomann 330 metronomes. Initially we bought ten pieces, but finally we selected six metronomes, so that their natural ticking frequencies for the 192 BPM marked frequency could be as similar as possible. For the experiments we fixed all the metronomes at this 192 BPM nominal frequency. We have chosen this frequency because in previous experiments [13] we found excellent synchronization for this nominal frequency value. Naturally, since there are no two identical units, in experiments
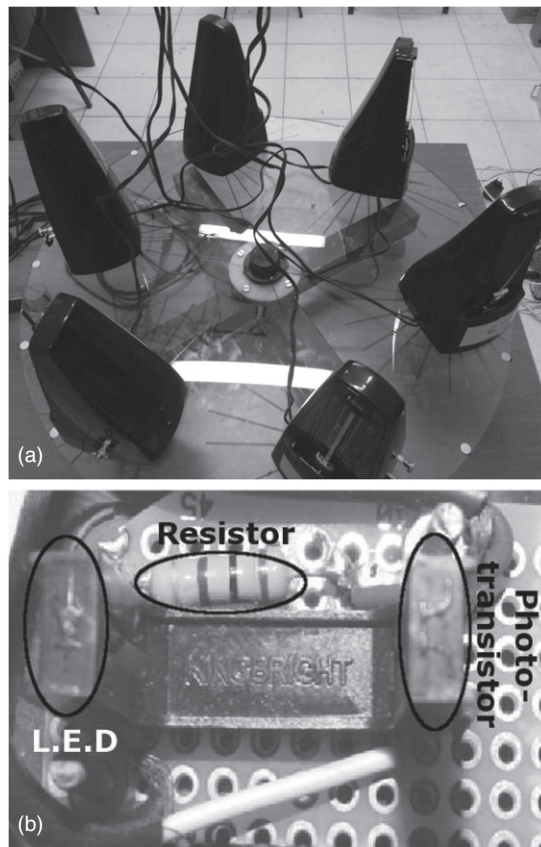
Figure 4. (a) Experimental setup, with the metronomes placed on the disc and the wiring that carries the information on the position of the metronomes' phases. (b) One of the light gates (Kingbright KTIR 0611 S) used for detecting the position of a metronome's bob. It is composed of an infrared LED and a phototransistor.

we have to deal with a non-zero standard deviation of their real natural frequencies and synchronization will not appear without a coupling mechanism.

One can easily check this by blocking the motion of the platform. Although the nominal frequencies are identical in this case, due to tiny differences in the real frequency values, one never observes a spontaneous synchronization of the beats.

In order to separately monitor the dynamics of all of the metronomes, photocell detectors (figure 4(b)) were mounted on them. These detectors are commercial ones (Kingbright KTIR 0611 S [15], available for purchase from many distributors, for example Transfer Multisort Elektronik [16]), and contain a light emitting diode and a phototransistor. They were mounted on the bottom of the metronomes, in the bob's movement plane.

The wires from each metronome (seen in figure 4) connect the photocells to a circuit board, allowing data collection through the USB port of a computer. For data collection we used a free, open-source program called *MINICOM*, which saves the collected data in log files [17]. Our setup is able to monitor the states of up to eight metronomes simultaneously. To reduce the data flow, the circuit board is programmed in such a manner that data are sent only when there is a change in the signal from the photocell system (i.e. a metronomes' bob passes the light gate). At such moments it sends a string like: $0 - 1 - 1 - 0 - 1 - 0$ 1450.
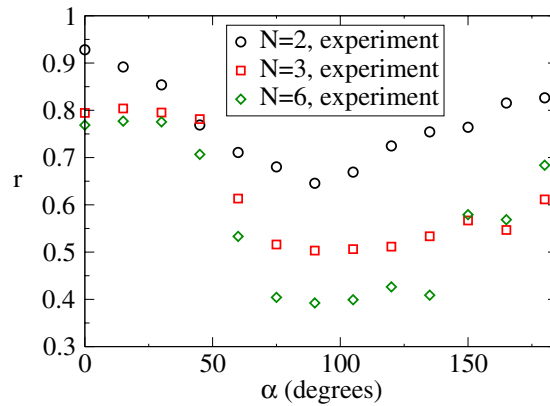
Figure 5. Experimental results for the synchronization level of the metronome system for several orientations of the metronomes on the disc. The averaged Kuramoto order parameter is plotted as a function of the α angle characterizing the metronomes' orientation on the platform. Different symbols correspond to different metronome numbers on the disc, as indicated in the legend.

The first six numbers characterize the metronome bobs' position relative to the photocell (whether the gate is open or closed) and the seventh number shows the time moment, where one time unit corresponds to 64 μs. Some additional steps are required in order to approximate the θ_j phases of all metronomes and to compute them for given time moments using the Kuramoto order parameter.

As a first step we must exclude from the data those moments when the metronome's bob returns and passes the second time through the light gate in one period. After this is done, in a second step we calculate the period of each cycle, and interpolate this time interval for the θ_j phases between 0 and 2π (corresponding to the state of a Kuramoto rotator) assuming uniform angular velocity. In such a manner, the θ_j phase of each metronome (considered here as a rotator) will be uniquely determined for each time moment, and the Kuramoto order parameter (2) is computed. All the presented results are averaged for ten independent experimental realizations. Experiments were carried out for two, three and six metronomes. The averaged results for the Kuramoto order parameter as a function of the α orientation angle of the metronomes is plotted on figure 5.

The curves suggest an order–disorder-type phase transition around $\alpha \approx 50°$. The transition from the partially synchronized state to an unsynchronized one appears as a result of the decreased coupling strength: $p_\perp = p \cdot \cos(\alpha)$. In agreement with the expected finite-size effects, by increasing the number of metronomes on the disc, sharper and sharper transition curves are observable. Going over $\alpha = 90°$, the $p_\perp$ component increases again. However, in parallel with this increase, the metronome's bob gets closer to the rotation axis of the disc, leading to a decrease in the torque produced by the $p_\perp$ pulse. The combined result of these two opposite effects will lead to a less evident second transition. It is worth noting that for the $\alpha \in [0°, 90°]$ interval both effects weakened the coupling, hence a sharper transition was observable.

4. Theoretical model

Inspired by the model described in [18], it is possible to consider a realistic model for the coupled metronome system. In this model we represent the metronomes by a rigid box containing a physical pendulum, as sketched in figures 6(a), (b). These boxes are placed
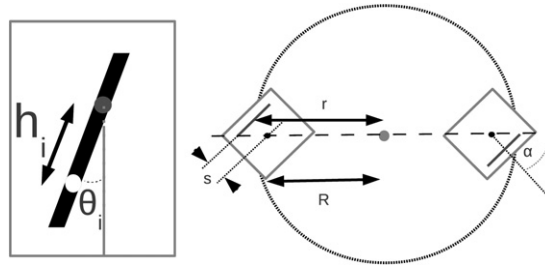
Figure 6. (a) Schematic view and notations for the considered mechanical model. The white dot denotes the centre of mass of the physical pendulums and the grey dot is the suspension axis. (b) A view from the top of the system with two metronomes (boxes represents the metronomes), the black point inside the box is the centre of mass of the metronome and the black line inside the box is the pendulums' swinging plane.

equidistant from each other on the perimeter of the disc, so that the swinging plane of the metronome forms an angle of $90° - \alpha$ with the radial direction on the disc (figure 6(b)).

In the reference frame of the Earth, the Lagrangian for such a system without damping and driving forces can be written as

$$L = \frac{J}{2}\dot{\phi}^2 + \sum_{i=1}^{N} \frac{m_i}{2} \left\{ \left[\frac{d}{dt}(x_i \cos\alpha_i + h_i \sin\theta_i) \right]^2 + \left[\frac{d}{dt}(x_i \sin\alpha_i) \right]^2 \right.$$

$$\left. + \left[\frac{d}{dt}(h_i \cos\theta_i) \right]^2 \right\} + \sum_{i=1}^{N} \frac{J_i \omega_i^2}{2} - \sum_{i=1}^{N} m_i g h_i (1 - \cos\theta_i). \tag{4}$$

The first term is the kinetic energy of the platform, the second one is the total kinetic energy for all of the pendulums' centre of masses, the third one is the total rotational kinetic energy of the pendulums around their centre of masses, while the last term is the total gravitational potential energy of all of the pendulums' centre of masses. The following notations are used: the index i labels the pendulums, J is the moment of inertia of the platform with the metronomes on it—taken relative to the vertical rotation axis passing through the centre of the platform, ϕ is the angular displacement of the platform, m_i is the total mass of the pendulum i ($m_i \approx W_1^{(i)} + W_2^{(i)}$, and we neglect the mass of the pendulum's rod), x_i is the horizontal displacement of the pendulum's suspension point due to the rotation of the platform, α is the orientation of the metronome's swinging plane, h_i is the distance between the pendulum's suspension point and their centre of mass, θ_i is the displacement angle of the ith pendulum relative to the vertical direction, J_i is the moment of inertia of the pendulum relative to its centre of mass and ω_i is the angular velocity for the rotation of the pendulum relative to its centre of mass. We assume that the distance between the centre of mass of the metronome and the centre of the disc is R, and this value remains constant, independent of α_i. (We remark that the centre of mass of the metronome is not in the pendulum's swinging plane. The heaviest part of the system is the driving mechanism, and in our simple model we assume that the position of this part remains unchanged when we rotate the metronome by an angle α.) One can immediately realize that $x_i = r_i \phi$, where $r_i = R + s_i \cdot \cos\alpha$ and s_i is the distance between the pendulum's swinging plane and the centre of mass of the metronome. Also, it is obvious that $\omega_i = \dot{\theta}_i$. We assume that the mass of all the weights suspended on the bobs are the same ($W_1^{(i)} = w_1$, $W_2^{(i)} = w_2$, and consequently $m_i = m$), and consider also $\alpha_i = \alpha$. Neglecting the $m_i g h_i$ constant terms, one obtains:

$$L' = \left(\frac{J + NmR^2}{2}\right)\dot{\phi}^2 + \sum_i \left(\frac{mh_i^2}{2} + \frac{J_i}{2}\right)\dot{\theta}_i^2$$
$$+ mr\dot{\phi}\cos\alpha \sum_i h_i\dot{\theta}_i\cos\theta_i + mg\sum_i h_i\cos\theta_i. \tag{5}$$

The Euler–Lagrange equations of motion yield:

$$(J + NmR^2)\ddot{\phi} + mr\cos(\alpha)\sum_i h_i[\ddot{\theta}_i\cos\theta_i - \dot{\theta}_i^2\sin\theta_i] = 0 \tag{6}$$

$$[mh_i^2 + J_i]\ddot{\theta}_i + mr\cos(\alpha)\ddot{\phi}h_i\cos\theta_i + mgh_i\sin\theta_i = 0. \tag{7}$$

These equations are valid for an ideal conservative system, where frictions and excitations are absent. Friction and excitation should thus be added separately:

$$(J + NmR^2)\ddot{\phi} + mr\cos(\alpha)\sum_i h_i[\ddot{\theta}_i\cos\theta_i - \dot{\theta}_i^2\sin\theta_i] + c_\phi\dot{\phi} + \cos(\alpha)\sum_i \mathbb{M}_i = 0 \tag{8}$$

$$[mh_i^2 + J_i]\ddot{\theta}_i + mr\cos(\alpha)\ddot{\phi}h_i\cos\theta_i + mgh_i\sin\theta_i + c_\theta\dot{\theta}_i = \mathbb{M}_i. \tag{9}$$

In the above equations of motion c_ϕ and c_θ are coefficients characterizing the friction in the rotation of the platform and pendulums, respectively. $\mathbb{M}_i$ are instantaneous excitation terms defined as

$$\mathbb{M}_i = M\delta(\theta_i)\dot{\theta}_i, \tag{10}$$

where δ denotes the Dirac function and M is a fixed parameter characterizing the driving mechanism of the metronomes. The choice of the form for $\mathbb{M}_i$ in equation (10) means that excitations are given only when a metronome's bob passes the $\theta = 0$ position. The term $\dot{\theta}$ is needed in order to ensure a constant momentum input, independent of the metronomes' amplitude. It also ensures that the excitation is given in the correct direction (direction of the motion). It is easy to see that the total momentum transferred, $\mathbb{M}_{\text{trans}}$, to the metronomes in a half period $(T/2)$ is always M:

$$\mathbb{M}_{\text{trans}} = \int_t^{t+T/2} M\delta(\theta_i)\dot{\theta}_i \, dt = \int_{-\theta_{\text{max}}}^{\theta_{\text{max}}} M\delta(\theta_i) \, d\theta_i = M.$$

This driving will be implemented in the numerical solution as

$$\mathbb{M}_i = \begin{cases} M/dt & \text{if } \theta_i(t - dt) < 0 \text{ and } \theta_i(t) > 0 \\ -M/dt & \text{if } \theta_i(t - dt) > 0 \text{ and } \theta_i(t) < 0 \\ 0 & \text{in any other case} \end{cases}$$

where dt is the time step in the numerical integration of the equations of motion. It can be immediately realized that this driving leads to the same total momentum transfer, M, as the one defined by equation (10).

The coupled system of equations (8) and (9) can be written in a more suitable form for numerical integration:

$$\ddot{\phi} = \frac{mr\cos(\alpha)\sum_i h_i\dot{\theta}_i^2\sin\theta_i - c_\phi\dot{\phi} - \cos(\alpha)\sum_i \mathbb{M}_i + A + B - C}{D}, \tag{11}$$

$$\ddot{\theta}_i = \frac{\mathbb{M}_i - mr\cos(\alpha)\ddot{\phi}h_i\cos\theta_i - mgh_i\sin\theta_i - c_\theta\dot{\theta}_i}{mh_i^2 + J_i} \tag{12}$$

where

$$A = m^2 g r \cos(\alpha) \sum_i \frac{h_i^2 \sin\theta_i \cos\theta_i}{mh_i^2 + J_i},$$

$$B = mrc_\theta \cos(\alpha) \sum_i \frac{h_i \dot\theta_i \cos\theta_i}{mh_i^2 + J_i},$$

$$C = mr \cos(\alpha) \sum_i \frac{h_i M_i \cos\theta_i}{mh_i^2 + J_i},$$

$$D = \left[J + NmR^2 - m^2 r^2 \cos^2(\alpha) \sum_i \frac{h_i^2 \cos^2\theta_i}{mh_i^2 + J_i} \right].$$

Taking into account that the metronomes' bobs have the shape sketched in figure 3 and the L_1 distances are fixed, the h_i and J_i terms of the physical pendulums in our model will be calculated as:

$$h_i = \frac{1}{w_1 + w_2} \left(w_1 L_1 - w_2 L_2^{(i)} \right) \tag{13}$$

$$J_i = w_1 L_1^2 + w_2 \left(L_2^{(i)} \right)^2. \tag{14}$$

Equations (11) and (12) are numerically integrated using a velocity Verlet-type algorithm. It was shown that a time step of d$t = 0.01$ s is sufficient to get good convergence. In order to characterize the synchronization level in the system, we used the classical Kuramoto order parameter, r, defined in section 2.

5. Model parameters

The parameters in our theoretical model were chosen in agreement with the characteristic values of our experimental device: $w_1 = 0.025$ kg, $w_2 = 0.0069$ kg, $L_1 = 0.0358$ m, $L_2 = 0.029$ m, $R = 0.27$ m, $s = 4$ cm and $J \in \{0.0729, 0.10935, 0.2187\}$ kg m^2 depending on the number of metronomes placed on the platform.

The damping and excitation coefficients were estimated from simple experiments. For the estimation of the c_θ value, a single metronome was considered on a rigid support. Switching off the excitation mechanism, a quasi-harmonic damped oscillation of the metronome took place. The exponential decay of the amplitude as a function of time uniquely defines the damping coefficient, hence a simple fit of the amplitude as a function of time allowed the determination of c_θ. Switching the exciting mechanism on leads to a steady-state oscillation regime with a constant amplitude. Since c_θ has already been measured, this amplitude is now uniquely defined by the excitation coefficient M. Solving equations (8) and (9) for a single metronome and tuning it until the same steady-state amplitude is obtained as in the experiments makes the estimation of M possible. Now that both c_θ and M are known, the following scenario is considered: all the metronomes are placed on the platform and synchronization is reached. In such a situation the platform has a constant amplitude oscillation. The angular amplitude of this oscillation will determine the c_ϕ damping coefficient. Its value is tuned by solving the equations (8) and (9), so that the experimentally observed amplitude of the disc's oscillations are reproduced. By performing these simple experiments all model parameters are realistically determined. The following parameter values were estimated: $c_\theta = 5 \times 10^{-5}$ kg m^2 s^{-1}, $c_\phi = 10^{-5}$ kg m^2 s^{-1} and $M = 6 \times 10^{-4}$ Nm s^{-1}.

One should also take into account the differences in the metronomes' natural frequencies, i.e. their non-zero standard deviation, σ. For the used 192 BPM nominal frequency value,
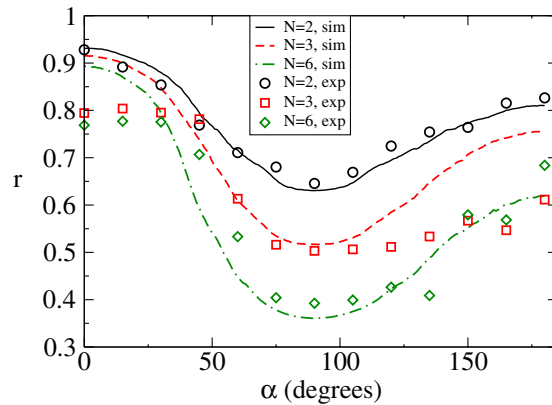
Figure 7. Comparison between the experimental and simulated results for the Kuramoto order parameter. As indicated in the legend, lines correspond to the simulated results and symbols correspond to the experimental results.

our metronomes had a non-zero standard deviation in their natural frequencies. In order to introduce these differences into the simulation, we added a noise in the L_2 terms. This leads to slightly different h_i values, in agreement with equation (13). The magnitude of the noise was chosen in such a manner that the standard deviations of the metronomes in the simulation were as close as possible to the experimental values.

6. Simulation results

Simulations were done for α values between $0°$ and $180°$, varying α with a step of $1°$. For better statistics we averaged the results of 100 independent simulations for each α value, using randomly chosen initial conditions. The results obtained for $N = 2, 3, 6$ metronomes allowed us to test our model and directly compare the results with the experimental data. For this comparison we have chosen the natural frequencies of the metronomes as close as possible to the experimentally measured values for the used metronomes. This means that the standard deviation σ of the natural frequencies is always adjusted close to the experimentally determined value. Comparison between the experimental and simulation results is done in figure 7.

Apart from the case when the system is composed of three metronomes, the experimental and theoretical results are in good agreement. Differences in the three metronome case are due to the fact that for three metronomes and $\alpha \in [90°, 180°]$ experiments have shown that in many cases one metronome beats in anti-phase with the others. This is less frequently reproduced in the simulations, leading to a higher order parameter value.

Fixing now the standard deviation for the metronomes as close as possible to the experimentally determined value for the ensemble of all six metronomes ($\sigma = 6.7 \times 10^{-7}$ BPM), we have investigated in more detail the Kuramoto-type phase transition for much larger metronome numbers, considering systems with up to $N = 100$ units. These studies allow a better illustration of the finite-size effects. For the 100 independent simulations realized at the same α value, the standard deviation σ_r of the r order parameter is also computed. Plotting $\sigma_r(\alpha)$ allows an excellent illustration of the increased fluctuations in the neighbourhood of the phase transition point. Results are plotted in figure 8.
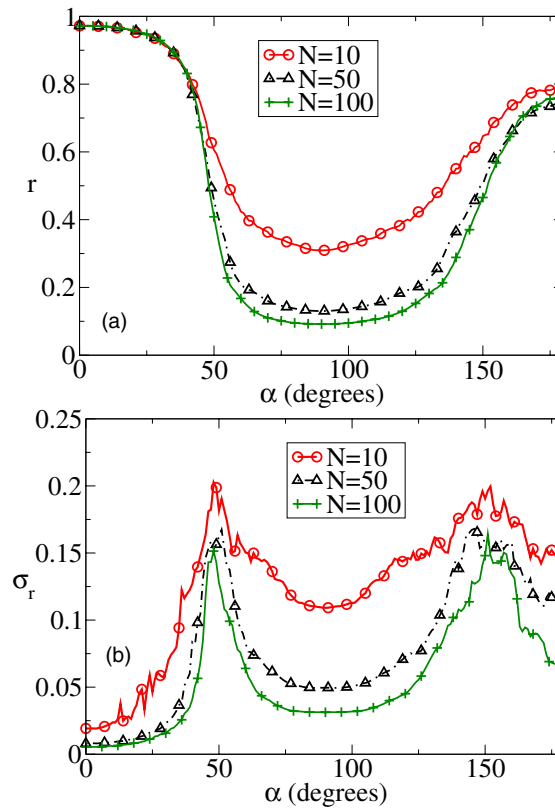
Figure 8. Simulation results for different numbers of metronomes on the disc. Each simulation point is the average of 100 simulations with randomly chosen initial conditions. (a) The synchronization order parameter as a function of the metronomes' orientation. (b) The fluctuation of the order parameter as a function of the metronomes' orientation on the disc.

In agreement with our expectations for larger systems, a sharper transition is observed. Fluctuations of the order parameter are also increased for larger system sizes. One can note again the asymmetric nature of the curves for the $\alpha \in [0°, 90°]$ and $\alpha \in [90°, 180°]$ intervals.

7. Summary

A globally coupled mechanical oscillator system consisting of metronomes placed on a freely rotating disc was investigated and used to illustrate the Kuramoto-type phase transition. Displacing the metronomes on the perimeter of the disc, the free rotation of the platform induces global coupling between them. By tilting the swinging plane of the metronomes relative to the radial direction on the disc, the coupling strength is finely tuned. As a function of the coupling strength, the system shows an order–disorder-type phase transition, similar to the one known in the Kuramoto model. For strong coupling, in-phase synchronization is observed. As the coupling strength is decreased, the spontaneous synchronization disappears. Finite-size effects can also be exemplified in this system. As the number of metronomes on the rotating platform is increased, sharper transitions are observable. A realistic theoretical model was considered in order to better understand the emerging collective behaviour in this system. The model was capable of reproducing the experimental results, and allowed the study

of systems with much larger number of metronomes, where a sharper transition in the order parameter is observed.

Instead of a rotating disc, the experiments can also be realized on a simple platform placed on two parallelly oriented cylinders that can freely roll on a table, as it is sketched in the work of Pantaleone [10]. The coupling will be controlled again by tilting the swinging plane of the metronomes relative to the axis of the cylinders. However, the advantage of using a rotating platform is that it does not require precise alignment of the cylinders, making the setup more robust and easier to use in classroom demonstrations. On the rotating platform the coupling can be also adjusted by manipulating the R distance (figure 2). We considered this scenario too, and found that the great disadvantage of this method is that one cannot reduce the coupling to zero due to the finite size of the metronome boxes.

Many additional classroom experiments can be done as a continuation of this study. One can investigate what happens if we change the metronomes' nominal beat frequencies or the metronomes' physical parameters. Also, one can investigate the system when external periodic driving is imposed. Studies can be done both on the experimental setup and/or by numerically simulating the presented realistic model.

Acknowledgments

References

[1] Strogatz S 2003 *Sync: The Emerging Science of Spontaneous Order* (New York: Hyperion)
[2] Kuramoto Y and Nishikawa I 1987 Statistical macrodynamics of large dynamical systems case of a phase transition in oscillator communities *J. Stat. Phys.* **49** 569
[3] Mirollo R and Strogatz S 1990 Synchronization of pulse-coupled biological oscillators *SIAM J. Appl. Math.* **50** 1645
[4] Bottani S 1996 Synchronization of integrate and fire oscillators with global coupling *Phys. Rev.* E **54** 2334
[5] Strogatz S 2000 From Kuramoto to Crawford: exploring the onset of synchronization in populations of coupled oscillators *Physica* D **143** 1–20
[6] Neda Z, Nikitin A and Vicsek T 2003 Synchronization of two-mode stochastic oscillators: a new model for rhythmic applause and much more *Physica* A **321** 238
[7] Huygens C 1665 Letter to de Sluse *Oeuveres completes de Christian Huygens* (La Haye: Societe Hollandaise Des Sciences) Letters nos 1333, 1335 and 1345
[8] Kapitaniak M, Czolczynski K, Perlikowski P, Stefanski A and Kapitaniak T 2012 Synchronization of clocks *Phys. Rep.* **517** 1–69
[9] Winfree A T 1967 Biological rhythms and the behavior of coupled oscillators *J. Theor. Biol.* **16** 15
[10] Pantaleone J 2002 Synchronization of metronomes *Am. J. Phys.* **70** 992–1000
[11] van der Pol B 1927 Forced oscillators in a circuit with non-linear resistance *Phil. Mag.* **3** 65–80
[12] Ulrichs H, Mann A and Parlitz U 2009 Synchronization and chaotic dynamics of coupled mechanical metronomes *Chaos* **19** 043120
[13] Tyukodi B, Boda Sz, Néda Z and Tunyagi A 2013 The rhythm of coupled metronomes *Eur. Phys. J.* B **86** 263
[14] Metronomes (Wikipedia) https://en.wikipedia.org/wiki/Metronome (accessed 14 July 2013)
[15] Kingbright photo interrupter www.tme.eu/en/Document/92b21f3f26b6948910585b1e34d6ef32/KTIR0911S.pdf, (accessed 16 July 2013)
[16] Transfer Multisort Electronik (company homepage) www.tme.eu/ (accessed 16 July 2013)
[17] Minicom http://alioth.debian.org/projects/minicom/ (accessed 14 July 2013)
[18] Czolczynski K, Perlikowski P, Stefanski A and Kapitaniak T 2009 Clustering and synchronization of *n* Huygens clocks *Physica* A **388** 5013–23